ROBOT MANIPULATOR DRIVE FAULT DIAGNOSTICS USING DATA-DRIVEN AND ANALYTICAL MODELLING

Michael Lipsett[1], Anthony Maltais[1], Mohammad Riazi[2],
Nicolas Olmedo[1], Osmar Zaiane[2]
[1]Department of Mechanical Engineering
[2]Department of Computing Science
University of Alberta
Edmonton, AB T6G 1H9
Michael Lipsett (780)-492-9494

Abstract: Belt-driven mechatronic systems are popular for a range of applications. A modified robotic manipulator was adapted to allow different belt-drive faults to be incorporated into the mechanism, with additional sensors to characterize the compromised kinematics. Different data-driven models were used studied to detect anomalies in motor power consumption and end-effector motion; and a physics-based, lumped-parameter dynamic model was used to identify different faults. Comparative assessment metrics were sdused to compare the performance of different fault models from sets of laboratory test data.

Key words: Machinery diagnostics; fault detection; machine learning; modelling; robotics; analytics; belt drives, time-varying systems.

1. INTRODUCTION

Mechatronic systems are increasingly popular in a range of products to improve quality and production in a variety of different ways. Many mechatronic devices use belt-driven power transmission systems. Improved understanding of the failure modes and effects in belt drives would enable diagnostic and prognostic techniques for predictive maintenance. Diagnostic models can be based on an understanding of the physics of the system and the effects of progressing component failure, or on data collected from systems that incorporate the component of interest under a range of operating conditions.

Physics-based models are used to represent a system using differential equations [1]. Within these differential equations, a variety of variables can be included in the model to accurately define the state of the system. A few examples of these factors include material properties, degrees of freedom, environmental and equipment specifications. The physics-based model provides an approximation of the response of a system to these factors. If the system has many of these parameters known and are appropriately integrated into the governing equations of the system, it is possible to estimate the other parameters and thereby calibrate a model that is an accurate representation of the physical system. By using this model, a response that varies from normal operating conditions in a way that relates to a change in a component indicates a fault in the system. Such a model can be used to simulate the effect of faults that can occur in the system. Bartelmus et al. [2] showed a case study of a dynamic model for fault detection in a real-world mechanical system.

In industrial practice, fault diagnosis and maintenance are generally done based on the knowledge and expertise of the people working with the equipment [3]. From observable signs of damage or an understanding of the rate at which wear-out occurs, maintainers perform repairs based on condition or schedule. Process and condition monitoring datasets allow diagnostics to be automated, using data to determine what normal operating conditions are (with normal variability or even time-varying behaviour for non-steady state systems) and comparing new data to assess whether there is a system fault. A drawback of this method is that an observer is limited to the information that is available from sensors. Determining the appropriate type, number, and locations is critical for observing features that correlate well to developing faults [4].

Faults can affect the system subtly, making them difficult to identify in the presence of other system effects and noise. The premise of data-driven diagnostics is that it is possible to observe features of faults of interest. The purpose of this study is to demonstrate the use of classical mechanical models and data driven analytical models on a robotic manipulator drive system operating cyclically under time-varying load.

There are many ways that a belt-driven system can change over its operating lifetime. Examples of common faults include: belts that become loose or are installed too tightly, rapid changes in temperature that may affect the materials, dust or debris build up in the track, and loose nuts along the body that introduce vibrations of components that aren't secured properly. Belts themselves are not instrumented in practice; but in this study, strain gauges were installed on the motor shaft to measure the torque output from the motor, and on a custom aluminum plate introduced into the belt itself to measure the tension directly. Using these measurements, it becomes possible to observe the effort of the motor under typical operating conditions and monitor how the systems changes when a fault is created in the system. This degree of observability allows the system to be characterized, and then the diagnostic performance of reduced observability can be assessed for different combinations of features are their relationships (by not using some measured data).

2. THEORY

This section presents the formulation of the governing equations for the laboratory-scale belt-driven system of interest, and introduces some candidate machine learning techniques for anomaly detection.

2.1 LUMPED-PARAMETER DYNAMIC MODEL FORMULATION FOR MOTOR AND BELT DRIVE

A custom planar belt-drive system with one actuator was designed and developed, with the motor, structure, and idlers illustrated in Figure 1. The mechanism moves in the horizontal plane, loaded with a mass that is supported on a flat plate by an unactuated wheel.
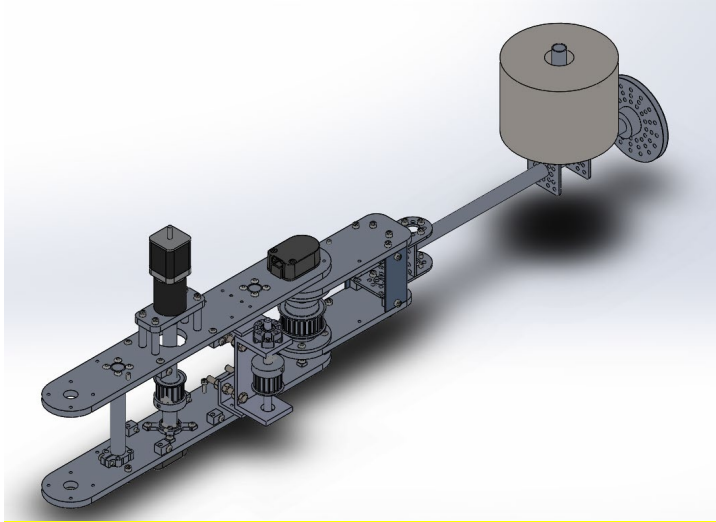
Figure 1: CAD Representation of Custom Belt-driven System (Belt Not Shown)

The robot manipulator belt drive contains three pulleys. There is a pulley attached to the motor to transmit power to the system, an adjustable idler pulley that is used to manipulate the tension in the belt and a pulley attached to a larger arm link that rolls on a steel surface. Nomenclature for variables and parameters for the governing equations are listed in Table 1.

Table 1: Nomenclature

r_m	Radius of the motor pulley
r_a	Radius of the arm pulley
r_i	Radius of the idler pulley
l_1	Center to center length on belt side 1
l_2	Center to center length on belt side 2
l_3	Center to center length on belt side 3
J_m	Polar moment of inertia of motor pulley
I_i	Mass moment of inertia of the idler pulley
I_a	Mass moment of inertia of the arm link
d_1	Effective damping coefficient of belt length 1
d_2	Effective damping coefficient of belt length 2
d_3	Effective damping coefficient of belt length 3
k_1	Effective stiffness coefficient of belt length 1
k_2	Effective stiffness coefficient of belt length 2
k_3	Effective stiffness coefficient of belt length 3
T_1	Tension in belt length 1

T_2	Tension in belt length 2	
T_3	Tension in belt length 3	
F_F	Coulomb friction force	
τ_m	Input torque from the motor	

It is assumed that there is stiffness and damping in the belt and each is a function of the belt length of each side. There are three degrees of freedom in this system, which are given by θ_m θ_i and θ_a. The governing equation for the motor pulley depends on tension forces from the belt, which are functions of their stiffening and damping properties across their respective lengths,

$$T_1 = k_1(\theta_i r_i - \theta_m r_m) + D_1(\dot{\theta}_i r_i - \dot{\theta}_m r_m) \tag{1}$$

$$T_3 = k_3(\theta_m r_m - \theta_a r_a) + D_3(\dot{\theta}_m r_m - \dot{\theta}_a r_a) \tag{2}$$

which yield the angular governing equation of motion:

$$\ddot{\theta}_m J_m = \dot{\theta}_i d_1 r_i r_m + \dot{\theta}_a d_3 r_a r_m - \dot{\theta}_m r_m^2(d_1 + d_3) + \theta_i k_1 r_i r_m + \theta_a k_3 r_a r_m - \theta_m r_m^2(k_1 + k_3) + \tau_m - F_{f_1} r_m \tag{3}$$

Similarly, the idler pulley, which is adjustable to tension the belt, has the following governing equation:

$$\ddot{\theta}_i I_i = \dot{\theta}_a d_2 r_a r_i + \dot{\theta}_m d_1 r_m r_i - \dot{\theta}_i r_i^2(d_2 + d_1) + \dot{\theta}_a d_2 r_a r_i + \theta_m k_1 r_m r_i - \theta_i r_i^2(k_2 + k_1) - F_{f_2} r_i \tag{4}$$

and the arm pulley, which is rigidly connected to the inertial load, is described by

$$\ddot{\theta}_a I_a = \dot{\theta}_m d_3 r_m r_a + \dot{\theta}_i d_2 r_i r_a - \dot{\theta}_a r_a^2(d_3 + d_2) + \dot{\theta}_m d_3 r_m r_a + \theta_i k_2 r_i r_a - \theta_a r_a^2(k_3 + k_2) - F_{f_3} r_a \tag{5}$$

The parameters for the analytical model are given in Table 2.

Table 2: Analytical Model Parameters

Parameter	Value	Units
r_m	0.0122	m
r_a	0.0122	m
r_i	0.0189	m
l_1	0.127	m
l_2	0.1524	m
l_3	0.1778	m
J_m	2.048E-9	m⁴
I_i	2.445E-6	kg-m⁴
I_a	0.5472	kg-m⁴
d_1	0.9460	kg/s
d_2	1.135	kg/s
d_3	1.324	kg/s
k_1	3.376E+5	N/m
k_2	4.051E+5	N/m
k_3	4.726E+5	N/m

The inertia parameters for the motor pulley and idler pulley were calculated directly using the approximation equations for polar and mass inertia of hollow cylinders. The calculation of inertia for the arm link was done using a 3D model in SolidWorks as seen in Figure 2. The mass moment of inertia was calculated about the center of mass and translated to the center of the pulley using the Parallel-axis Theorem.
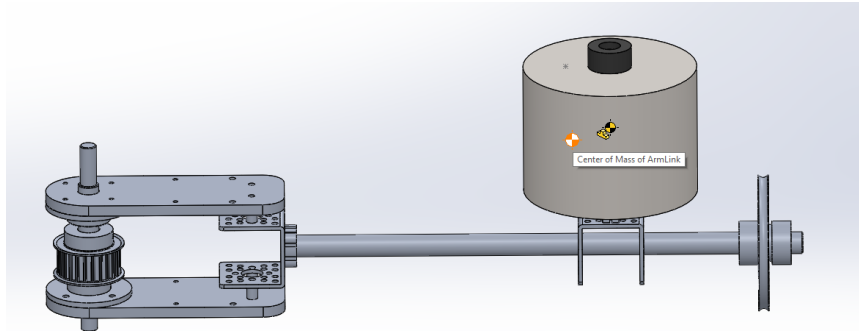

Figure 2: Arm and Driven Pulley with Support Idler

The effective inertias of the system are summarized in Table 3.

Table 3: Inertia Coefficients

Inertia Parameter	Value	Units
J_m	2.048E-9	m^4
I_i	2.445E-6	kg-m^4
I_a	0.5472	kg-m^4

The stiffness of each segment of the belt is a function of its length. A segment of belt of nominal length 0.163 m was loaded in an MTS machine to determine the stiffness per unit length at room temperature. Two trials were run, and the MTS machine generated load-displacement plots from which the average stiffness was calculated to be 43.3 kN/m. The stiffness was then scaled to determine the stiffness of the belts for each of the three lengths on the manipulator belt drive, as listed in Table 3.

Table 4: Stiffness Coefficients

	Length (m)	Stiffness, k (kN/m)
l_{test}	0.163	43.3
l_1	0.127	33.8
l_2	0.153	40.5
l_3	0.178	47.3

As with stiffness, the damping of the belt is a function of the length of each side. To determine the effects of damping in the belt, the 0.163 m specimen was half loaded in the MTS machine while the other side was attached to a small weight. The belt and weight were then lifted and released. The response of the belt for a typical trial is shown in Figure 3.
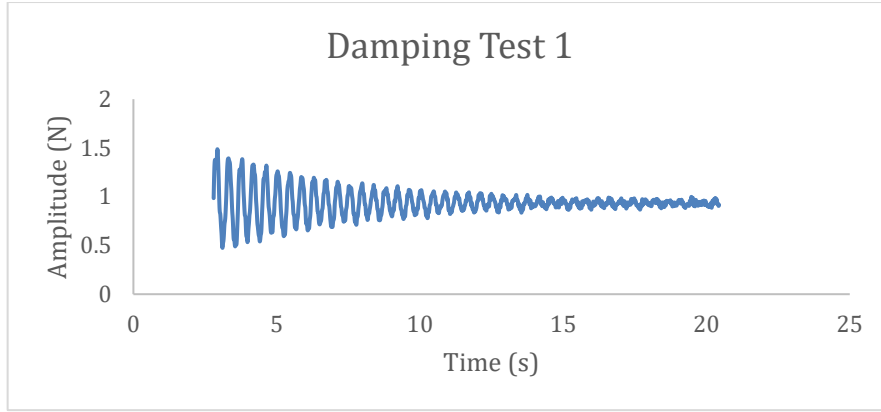
Figure 3: Decaying Exponential Response of Belt with Hanging Mass

By using the logarithmic decrement, the damping ratio ζ, can be calculated via:

$$\zeta = \frac{\delta}{2\pi} \tag{10}$$

The critical damping coefficient can be calculated via:

$$C_c = 2\left(\sqrt{k_{eff}m_{eff}}\right) \tag{11}$$

Finally, the damping coefficient, *d,* is calculated as

$$d = \zeta * C_c \tag{12}$$

As was done with the stiffness, the damping coefficient was scaled to the corresponding length of each side of the belt drive system. The results are given in in Table 5.

Table 5: Damping Coefficients

	Length (m)	Damping, *d* (kg/s)
l_{test}	0.163	1.121
l_1	0.127	0.946
l_2	0.152	1.135
l_3	0.178	1.324

The calibrated model can now be used to simulate dynamic behaviour from input of a non-conservative generalized force (motor torque) as a function of time. Differences between the simulation results and the response of an actual system are due to changes in the system dynamics (which may be faults), unmodeled dynamics, error in the model due to calibration, error in the simulation solution (solver type, step size, or implementation), or noise.

2.2   MACHINE LEARNING FOR PROGNOSTICS & HEALTH MANAGEMENT

Machine learning is a set of data analytical techniques that allow for the extraction of information from data that can help to accelerate the development of data-driven methods required in a prognostics and health management (PHM) system comprising of anomaly detection, diagnosis and prognosis methods. In general, a machine learning program can be used to "learn" from a measurable experience so that when such an experience happens again, it is recognized. In mechanical system diagnostics, a system that learns to recognize measurements of both regular operating conditions and anomalous operating conditions – and be able to tell the difference between the two.

Machine learning techniques can typically be categorized as supervised (data are labeled) and non-supervised techniques (data are un-labeled) [5]. Within these branches, there are many methods that can be used in detecting anomalies in a dataset. These include statistical methods, proximity-based methods, and deviation (or classification-based) methods.

Statistical methods assume that the data follows a specific distribution, and so the model can be created from a specified probability distribution [6]. By utilizing a probability distribution, anomalies can be detected by finding data that deviate dramatically from the distribution. Common statistical methods include Gaussian Mixture Models [7], various regression models, and Histogram-based Outlier Score models [8]. Some advantages and disadvantages are provided in Table 6.

Table 6: Statistical Methods

Advantages	Disadvantages
• If the underlying data distribution is correctly identified (assumed), these methods present a statistically proven solution for anomaly detection. • The resulting anomaly score is associated with a confidence interval. • Depending on the robustness of the distribution to anomalies within data, these methods can be used in an unsupervised fashion.	• Statistical methods assume that the data is from a specific distribution, which is normally not the case in a real world setting with high dimensional data. • Require a large sample of training data to estimate model parameters

Proximity, or cluster-based, methods for detecting data anomalies assume that similar data points can be "clustered" together. The more a data point has a certain characteristic, the closer it would appear to a parameter called a "cluster centroid". Therefore, anomalous data points can be determined by setting a threshold for its distance from a cluster centroid. These methods are typically categorized as unsupervised because they can be used to identify clusters of data points that are similar, without labels. Some commonly used cluster-based methods are k-means clustering [9] and self-organizing maps [10]. Some advantages and disadvantages of using proximity-based methods can be found in Table 7 below.

Table 7: Proximity Methods

Advantages	Disadvantages
• Can operate in an unsupervised fashion, without requiring any labeled data. • Capable of being used in incremental models, i.e., new data points. can be given and tested for anomaly. • Fast test time results due to testing against small number of identified clusters.	• Performance of these methods is very much dependent on the clustering algorithm and how successful they can identify the structure of normal data. • Some clustering methods force every data point to be part of a cluster. Hence, clustering methods that assume anomalies do not belong to clusters consider these as normal. • Some methods only work well if anomalies do not form smaller clusters amongst themselves.

Classification methods are used to classify test samples using a learned classifier by training on labeled datasets. The classifier learns by using the labeled training set which consists of labeled normal and anomalous operating conditions. It can then be tested on a second unlabeled dataset to determine the accuracy of the classifier in identifying normal and abnormal datapoints. Two commonly used classification methods are one-class support vector machines [11] and neural networks [12]. Some advantages and disadvantages of classification-based methods are given in Table 8.

Table 8

Advantages	Disadvantages
• Classification-based methods, particularly multi-class methods, can be used to distinguish between samples belonging to different normal classes. This can be useful with systems that have multiple normal operating conditions. • Test time computation is very fast due to the pre-trained model.	• Multi-class methods require accurate labeling of normal classes, which are often hard to acquire. • Some classification-based methods assign a class to samples. This may be a disadvantage as it does not provide a tangible anomaly score.

3. EXPERIMENT DESIGN

An experimental system was developed to produce a cyclical motion in a simple belt-driven system corresponding to the analytical model described above. The system was designed for reproducibility so that multiple experiments could be run and have similar results. The apparatus is shown in the photograph in Figure 4.
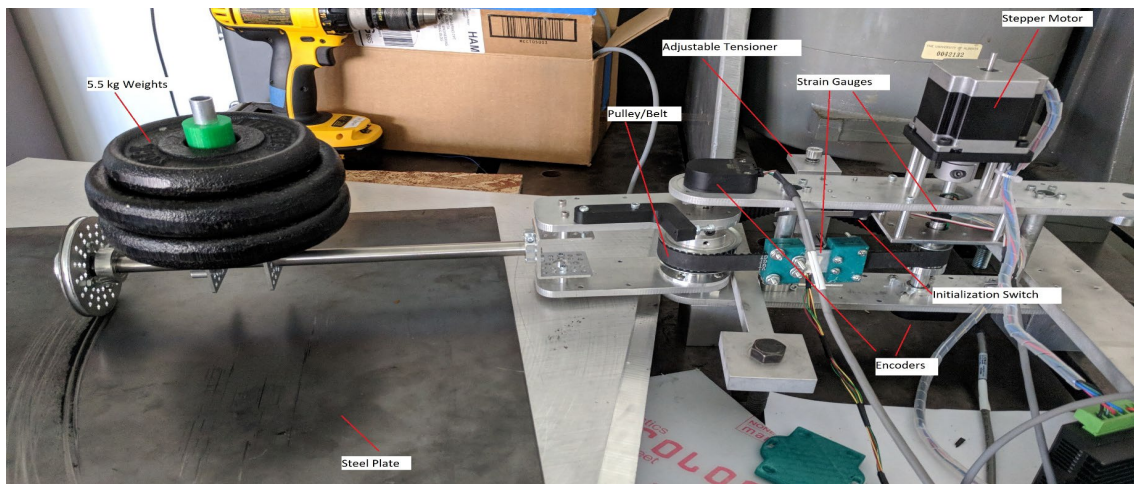

Figure 4: Side View of Arm Driven by Stepper through Belt Drive

Figure 5 shows the belt tension measurement ligament with strain gauges. A prismatic rectangular piece of aluminum is connected to the belt. A full-bridge strain gauge circuit measures the instantaneous tension in the belt, which is recorded by a microcontroller.
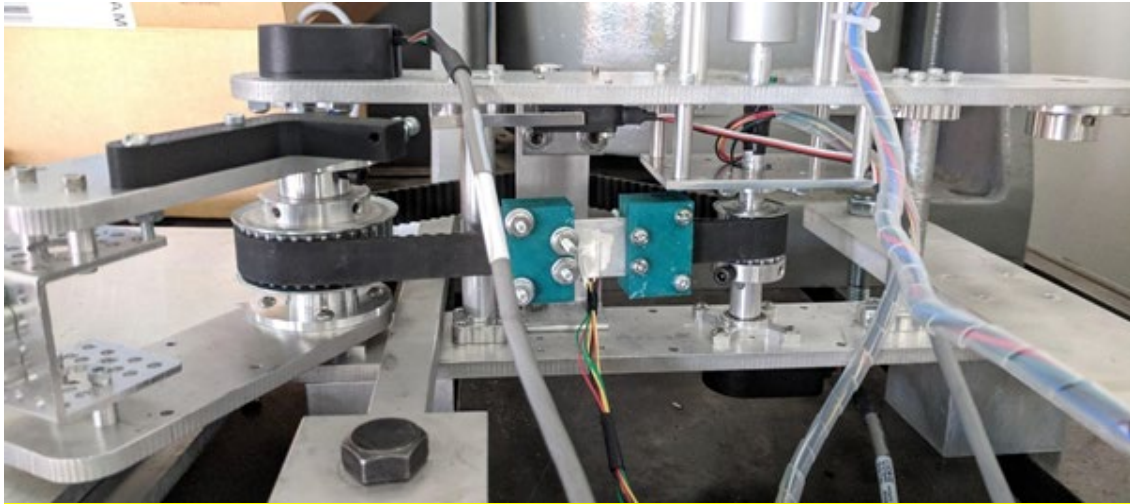
Figure 5: Belt Tension Measurement Sensor and Joint Sensor at Arm Base

Figure 6 shows a top view of the apparatus, with a second joint sensor that measures the arm motion (in addition to the sensor collocated on the motor shaft). Both are US Digital E2 optical encoders. A full-bridge strain gauge sensor measures torque on the motor shaft. A steel plate supports the 5.5 kg mass loading the aluminum idler at the end of the arm. Restraining clamps hold the base of the mechanism on a 3 tonne seismic platform. The drive train is fitted with an adjustable tensioning device mounted with an idler pulley, which allows the tension in the belt to be modified in different trials. The tensioner has four bolts that fasten it to the main body of the arm and the heights of the bolts can be changed to adjust the height of the idler pulley, increasing or decreasing the tension in the belt.

Figure 6: Top View of Apparatus

The system is controlled by a programmed Teensy 3.2 Microcontroller to actuate the motor and read the measurements from the instrumentation at a sampling rate of 100 Hz. The mechanism is actuated by a brushless stepper motor to drive the belt through a programmed range of motion (typically between 19 and 126 degrees). The motor is controlled by a Leadshine DM542 Microstep Drive. A switch on the arm is activated during the arm's first cycle. The switch tells the microcontroller that it has reached the starting point, after which the motor begins a looping script to move the arm in an oscillatory path (5 seconds counterclockwise, stop for 0.1 s, 5 s clockwise, 0.1 stop, and repeat for a preset number of cycles). The robot arm transmits power from the motor to the arm link via a timing belt and pulley system. The pulley on the shaft connected to the motor and the pulley on the adjustable tensioner are both 5GT 16-tooth pulleys; and the pulley on the joint is a 5GT 24-tooth pulley.

4. EXPERIMENTAL RESULTS

A set of cycles were run to do baseline trials of normal operating condition at a belt tension of the belt of 150 N. The torque profile over multiple cycles is shown in the plot in Figure 7.
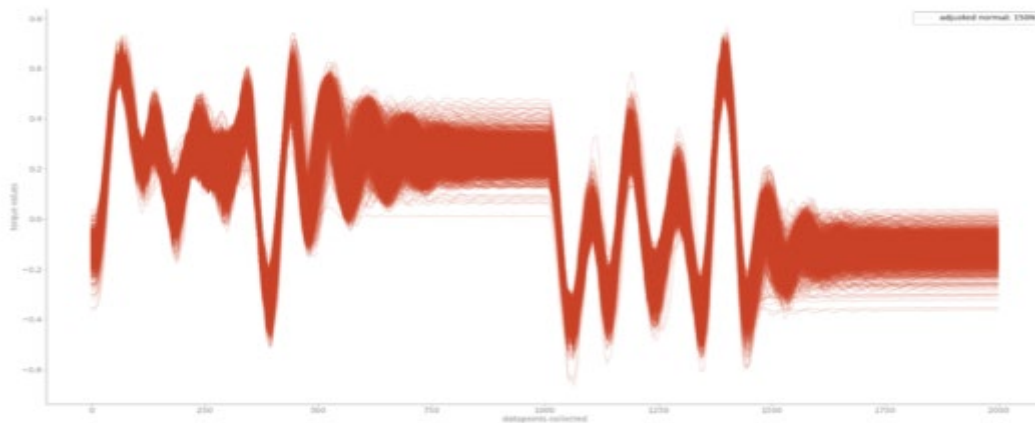

Figure 7: Normal Operation Torque Profile at 150 N Belt Tension

After a baseline torque profile was established, a variety of fault modes were individually tested on the system:

- **Loose Belt:** Using the tensioner mechanism and the instrumentation on the belt, the belt was able to be precisely loosened. The loose belt fault mode was tested at 100 N and 120 N.
- **Tight Belt:** Similarly, the belt was able to be tightened above the normal operating tightness. For this fault mode, the tension was set to 168 N.
- **Increased Friction/Sand Buildup:** For this fault mode, sand was scattered along the steel plate that the pulley was running along.
- **Extreme Temperature Change:** For this fault mode, the ambient temperature around the manipulator arm was measured by a thermocouple. The temperature was increased to approximately 40 degrees Celsius from room temperature using a heat lamp. It was observed that the belt contracted, resulting in a tension increase from 150 N to 168 N.

The experimental conditions for these fault modes are summarized in Table 9.

Table 9: Fault Modes and Number of Cycles per Trial

	TEMP	TENSION	NO. SAMPLES
Normal	~23.5	~150	7193 (22hrs)
Loose l1	~23.5	~120	182
Loose l2	~23.5	~99-100	180
Tight	~23.5	~168	194
High Temperature	~40-42	~166-169	210
Sand (friction)	~23.5	~150	183

Figure 8 on the following page shows the effects of these fault modes on the torque profile compared to the normal operating condition profile. It can be observed that while these are fault modes of the system, their impact affects the torque profile very subtly, meaning that they would be difficult to identify in a real-world system.
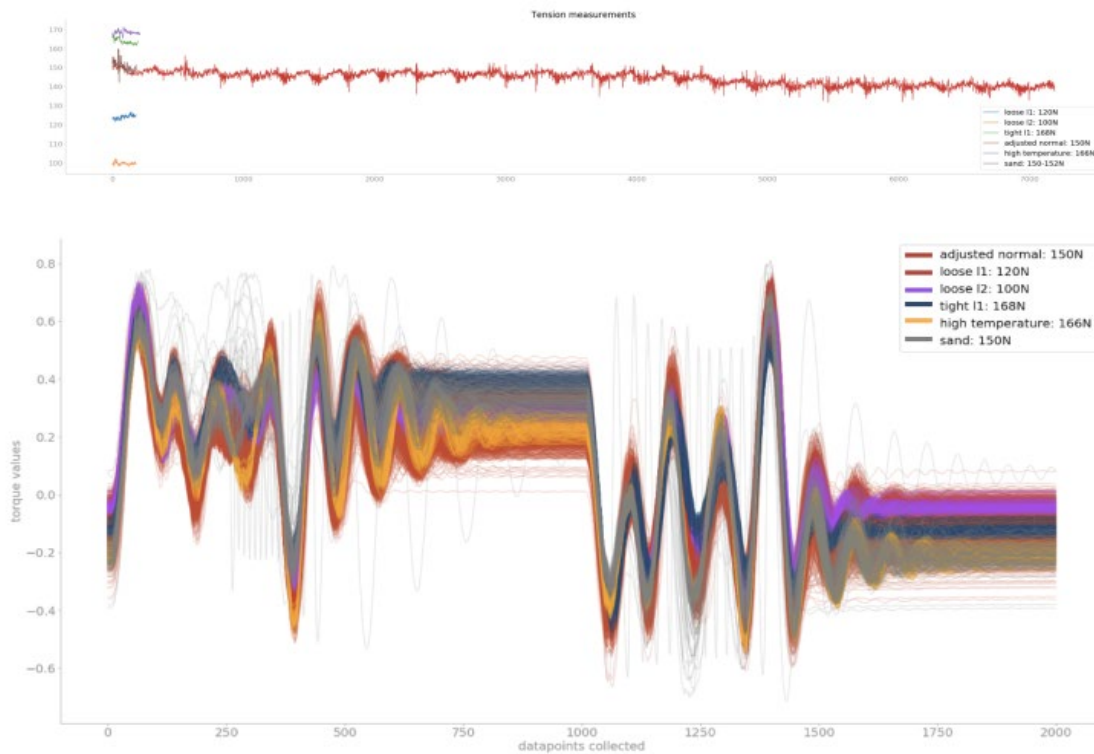
FUTURE WORK

Feature ranking and comparative assessment of a range of machine learning techniques are currently being analyzed. The anomaly detection and fault identification performance using machine learning methods will be compared with the goodness of fits for a set of physics-based models (normal, loose belt, tight belt, high friction).

ACKNOWLEDGMENTS

REFERENCES

[1]   Isermann, R. (2005). Model-based fault-detection and diagnosis – status and applications. *Annual Reviews in Control, 29*(1), 71-85. doi:10.1016/j.arcontrol.2004.12.002

[2]   W. Bartelmus, F. Chaari, R.Zimroz and M. Maddar, Modelling of gearbox dynamics under time-varying nonstationary load for distributed fault detection and diagnosis, "*European Journal of Mechanics-A/Solids, vol. 29, no.4, pp.637—646,2010.*

[3]   Potes Ruiz, Paula, Bernard Kamsu Foguem, and Bernard Grabot. "Generating Knowledge in Maintenance from Experience Feedback." *Knowledge-Based Systems*, vol. 68, 2014, pp. 4-20.

CrossRef, https://www.sciencedirect.com/science/article/pii/S0950705114000422, doi:10.1016/j.knosys.2014.02.002.

[4]   Ting-Hua Yi, Hong-Nan Li, and Ming Gu. "Optimal Sensor Placement for Health Monitoring of High-Rise Structure Based on Genetic Algorithm." *Mathematical Problems in Engineering*, vol. 2011, 2011, pp. 1-12.

 [5]   Sathya, R., and A. Abraham. "Comparison of Supervised and Unsupervised Learning Algorithms for Pattern Classification." *International Journal of Advanced Research in Artificial Intelligence*, vol. 2, no. 2, 2013, pp. 34–38., doi:10.14569/issn.2165-4069.

[6]   Clifton, David A., Peter R. Bannister, and Lionel Tarassenko. "A Framework for Novelty Detection in Jet Engine Vibration Data." *Key Engineering Materials*, vol. 347, 2007, pp. 305-310. CrossRef, doi:10.4028/www.scientific.net/KEM.347.305.

[7]   G. J. McLachlan and K. E. Basford, *Mixture models: Inference and applications to clustering.* Marcel Dekker, 1988, vol. 84

[8]   M. Goldstein and A. Dengel, \Histogram-based outlier score (hbos): A fast unsupervised anomaly detection algorithm," *KI-2012: Poster and Demo Track*, pp. 59-63, 2012.

[9]   J. MacQueen et al., \Some methods for classification and analysis of multivariate observations," in *Proceedings of the fifth Berkeley symposium on mathematical statistics and probability*, Oakland, CA, USA, vol. 1, 1967, pp. 281-297.

[10]   T. Kohonen, \The self-organizing map," *Proceedings of the IEEE*, vol. 78, no. 9, pp. 1464-1480, 1990.

[11]   J. Ma and S. Perkins, \Time-series novelty detection using one-class support vector machines," in *Neural Networks, 2003. Proceedings of the International Joint Conference on*, IEEE, vol. 3, 2003, pp. 1741-1745.

[12]   S. Hawkins, H. He, G. Williams, and R. Baxter, \Outlier detection using replicator neural networks," in *International Conference on Data Warehousing and Knowledge Discovery*, Springer, 2002, pp. 170-180.